

Cascadia subduction slab heterogeneity revealed by three-dimensional receiver function Kirchhoff migration

Cheng Cheng, Thomas Bodin, Benoit Tauzin, Richard M. Allen

► **To cite this version:**

Cheng Cheng, Thomas Bodin, Benoit Tauzin, Richard M. Allen. Cascadia subduction slab heterogeneity revealed by three-dimensional receiver function Kirchhoff migration. *Geophysical Research Letters*, American Geophysical Union, 2017, 44 (2), pp.694-701. 10.1002/2016GL072142 . hal-02329275

HAL Id: hal-02329275

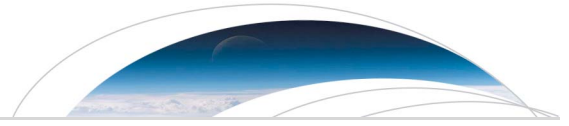
<https://hal-univ-lyon1.archives-ouvertes.fr/hal-02329275>

Submitted on 21 Sep 2021

HAL is a multi-disciplinary open access archive for the deposit and dissemination of scientific research documents, whether they are published or not. The documents may come from teaching and research institutions in France or abroad, or from public or private research centers.

L'archive ouverte pluridisciplinaire **HAL**, est destinée au dépôt et à la diffusion de documents scientifiques de niveau recherche, publiés ou non, émanant des établissements d'enseignement et de recherche français ou étrangers, des laboratoires publics ou privés.

Copyright



RESEARCH LETTER

10.1002/2016GL072142

Key Points:

- High-resolution seismic discontinuity structure of Cascadia subduction slab is imaged by 3-D receiver function Kirchhoff migration
- Primary and multiple arrivals in the final migration image are separated by comparison with synthetic results and a tomography model
- Slab heterogeneity along strike is interpreted as due to slab weakness, offshore hydration processes, and the presence of a plume

Supporting Information:

- Supporting Information S1
- Figure S1
- Figure S2

Correspondence to:

C. Cheng,
cchengster@berkeley.edu

Citation:

Cheng, C., T. Bodin, B. Tauzin, and R. M. Allen (2017), Cascadia subduction slab heterogeneity revealed by three-dimensional receiver function Kirchhoff migration, *Geophys. Res. Lett.*, *44*, 694–701, doi:10.1002/2016GL072142.

Received 2 DEC 2016

Accepted 4 JAN 2017

Accepted article online 5 JAN 2017

Published online 17 JAN 2017

©2017. American Geophysical Union.
All Rights Reserved.

Cascadia subduction slab heterogeneity revealed by three-dimensional receiver function Kirchhoff migration

Cheng Cheng¹ , Thomas Bodin² , Benoit Tauzin², and Richard M. Allen¹ 

¹Department of Earth and Planetary Science, University of California, Berkeley, California, USA, ²Laboratoire de Géologie de Lyon: Terre, Planètes et Environnement, Université de Lyon, Université Lyon 1 and Ecole Normale Supérieure de Lyon, Lyon, France

Abstract We present a 3-D model of upper mantle seismic discontinuity structure below Cascadia using a receiver function Kirchhoff migration method. A careful analysis of the primary and multiple reverberated phases allows imaging of the Juan de Fuca plate dipping below the North American continent. The subducting slab is observed as an eastward dipping signal at all latitudes. We associate this signal with a thermal gradient between the slab and surrounding mantle, rather than a sharp chemical discontinuity. Our model also shows along-strike variations in the dipping angle and strength of this signal. To the southern and northern ends of the subduction system, the signal is clearly observed down to ~300 km. However, beneath central Oregon, this structure is missing below ~150 km depth. We propose that this gap is due to weakening of the slab beneath central Oregon possibly caused by deformation and hydration combined with plume-slab interaction processes after subduction.

1. Introduction

The Cascadia subduction zone is a young lithosphere end-member of the global subduction system [Hacker *et al.*, 2003]. The Juan de Fuca plate that subducts beneath Cascadia is divided into two subplates: the Gorda section subducting under Northern California and the rest of the Juan de Fuca plate (JdF) subducting under Oregon and Washington. Contrary to older and colder subduction zones such as the western Pacific margins, the absence of a well-developed Wadati-Benioff zone in Cascadia limits direct observation of the top of this subducting slab [McCrorey *et al.*, 2012].

As one of the most well-observed subduction zones in the world, extensive seismic studies have been done in Cascadia. These include teleseismic tomography [e.g., Obrebski *et al.*, 2011; Hawley *et al.*, 2016], regional tomography [e.g., Gao, 2016; Bell *et al.*, 2016], receiver function imaging [Audet *et al.*, 2009, 2010], observations of seismic anisotropy [Martin-Short *et al.*, 2015], reflection imaging offshore [Han *et al.*, 2016], and seismicity studies [McCrorey *et al.*, 2012]. All these studies provide imperfect constraints on the geometry and physical properties of the subducting slab and surrounding mantle.

From teleseismic transmitted waves, Bostock *et al.* [2002] and Bostock [2013] showed that the dipping angle of the slab is around 30° in the uppermost 100 km of the mantle. Teleseismic tomography models [Burdick *et al.*, 2010; Obrebski *et al.*, 2010, 2011] showed that the dipping angle of the slab between 200 km and 600 km depth varies along strike with steeper angle to the south. In central Oregon, these models also showed the segmentation of the slab, interpreted as the interaction between the subducted plate and the Yellowstone mantle plume. At shallow depth, a recent study by Han *et al.* [2016] suggests variation of the hydration of oceanic crust/mantle along the strike of the subduction zone, based on the regional differences in the extent of crustal/mantle bend-faulting near the deformation front. They inferred that the oceanic plate offshore Oregon has a higher potential for crustal hydration and mantle serpentinization than offshore Washington.

Receiver function analysis resolves sharp velocity contrasts that produce conversions from *P* to *S* waves, which in turn can provide information on the chemical and thermal properties of the upper mantle. Previous receiver function (RF) studies of the North American continent [e.g., Levander and Miller, 2012; Tauzin *et al.*, 2013; Hansen *et al.*, 2015; Hopper and Fischer, 2015; Ford *et al.*, 2016] commonly utilize the Common Conversion Point (CCP) stacking method. However, this method assumes horizontal discontinuities and is known to give poor results in the case of dipping interfaces, such as in the Cascadia subduction zone

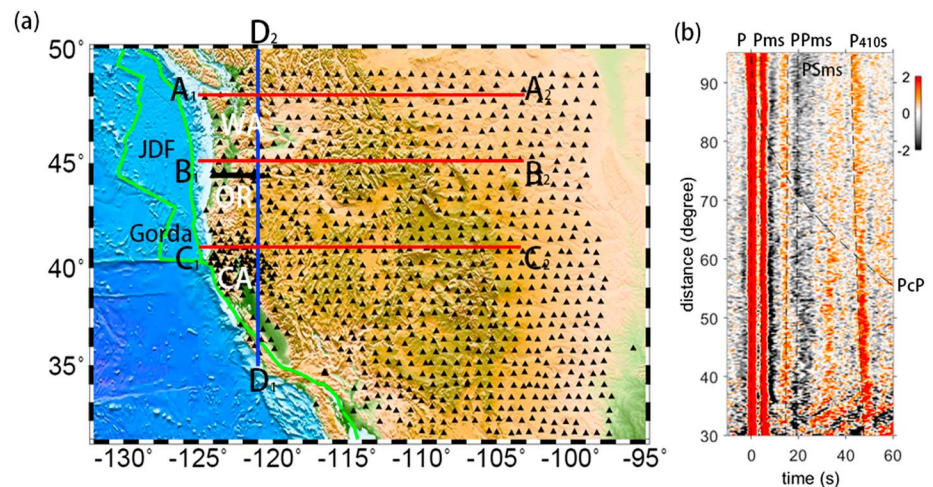


Figure 1. (a) Map of Western U.S. and broadband seismic stations (black triangles) used in this study. (b) Time-distance section for all the receiver functions used in this study. The primary signal (*Pms*) and later multiples are labeled.

[Rondenay, 2009; Cheng *et al.*, 2016]. Bostock *et al.* [2002] imaged the velocity structure of the subducting plate by using a more sophisticated migration/inversion scheme (the 2-D generalized Radon transform migration), but this method has been limited to 2-D slices because it requires dense arrays of instruments and intense computation in calculating the transform coefficient for the dense arrays. The position of the slab interface at depth, its seismic structure, and its lateral variations therefore remain controversial and seismologists keep on applying advanced imaging methods to reveal it [e.g., Tauzin *et al.*, 2016].

In this paper, we present an image of the Cascadia subduction zone extending (from 10 km down to 450 km depth, based on a 3-D prestack Kirchhoff depth migration (PKDM) method for teleseismic receiver functions [Cheng *et al.*, 2016]. We account for 3-D velocity variations to provide a more accurate and complete 3-D discontinuity model for the subducting slab than previous studies [Levander and Miller, 2012; Tauzin *et al.*, 2013]. We use a synthetic test to distinguish primary phases from multiple reflected phases that generate spurious artificial interfaces. We find that the dominant seismic discontinuity in the subducting plate, a dipping positive interface marking a shear-wave velocity increase with depth, varies anomalously from the Gorda to the rest of the Juan de Fuca portions of the plate. This heterogeneous pattern of seismic discontinuity structure inside the oceanic slab coincides potentially with slab-plume interaction inferred at similar depth [Obrebski *et al.*, 2010] and may also be related with the fluid distribution in the subducting plate, as reported by Han *et al.* [2016].

2. Data and Method

We use a receiver function (RF) database created by using three-component broadband records of passive seismicity at stations deployed during the U.S. Transportable Array experiment between January 2004 and November 2009 [Tauzin *et al.*, 2013]. Waveforms were obtained from the Incorporated Research Institutions for Seismology Data Management Center for 932 teleseismic earthquakes, which resulted in 64,578 receiver functions. The RFs were obtained by deconvolving the vertical component of seismic records from their radial component and using an iterative time domain deconvolution [Ligorria and Ammon, 1999].

Two denser arrays of stations were added [Tauzin *et al.*, 2016]: the Cascadia 93 and Mendocino experiments located in central Oregon and northern California, respectively (Figure 1a). The wide aperture Transportable Array allows us to image the western U.S. structure down to the transition zone across the continent. Two RF data sets were obtained from waveforms low-pass filtered at 0.1 and 0.2 Hz. In this work, we present a migrated model obtained at 0.2 Hz, but the same processing has been done from the 0.1 Hz data-set (see Figure S1 in the supporting information). A seismic section derived by stacking all the RFs at 0.2 Hz is shown in Figure 1b. The data are aligned on the *P* arrival and stacked within 0.25° epicentral distance intervals. After the direct *P* arrival at 0 s, clear arrivals with similar moveout (travel time decreasing with epicentral distance) are observed around 5 s and 50 s. These are, respectively, the direct *P*-to-*S* conversions

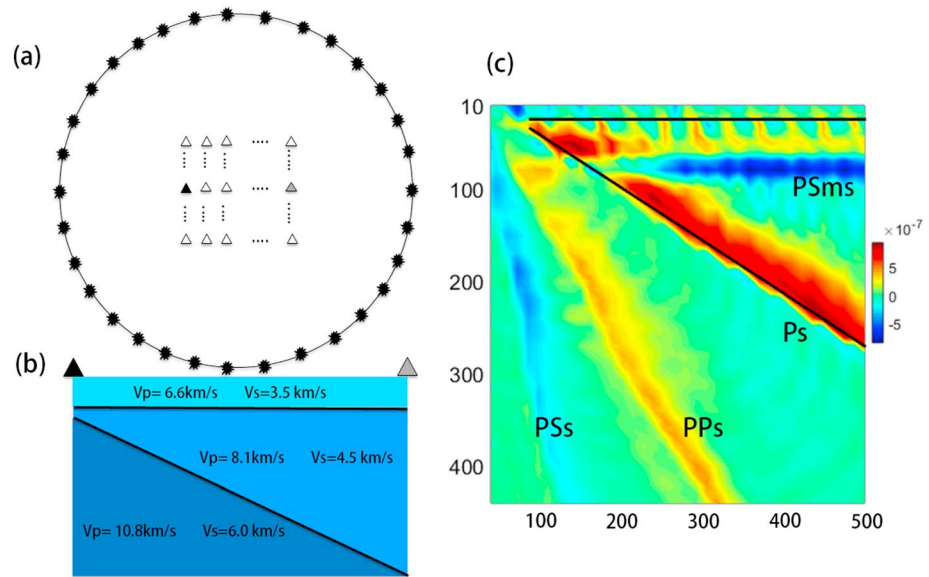


Figure 2. (a) Schematic figure (not to scale) showing the earthquake source distribution map used for synthetics. A circle of sources surrounds our grid of surface seismic stations (triangles), which is roughly 80° (epicentral distance) from the sources. (b) A vertical section through our synthetic velocity model. (c) The final migrated results using our Kirchhoff migration method. The solid black lines mark the real location of the model discontinuity. The primary signal and late multiples are labeled on the figures.

at the continental Moho (Pms), and the 410 km discontinuity ($P410s$) under the array. Figure 1b shows that the signal after the Pms is dominated by free-surface reflected multiples (travel time increasing with epicentral distance) in the crust, the $PPms$ (positive) and $PSms$ (negative) phases. Here “m” indicates that waves are transmitted or reflected from the continental Moho.

We use a 3-D prestack Kirchhoff depth migration (PKDM) method for the migration [Cheng et al., 2016]. This algorithm considers the effects of diffraction, scattering, and travel time alteration caused by 3-D volumetric heterogeneities. It is therefore particularly useful for imaging complex 3-D structures such as dipping discontinuities, which is hard to accomplish with traditional methods. Given a smooth 3-D reference model, travel times for P and S waves are computed with an efficient eikonal solver, the fast marching method [Rawlinson and Sambridge, 2004]. We also account for the elastic scattering patterns, where the amplitude of converted S waves depends on the angle between the incident P wave and the scattered S wave [Dahlen et al., 2000]. The reference P model in the mantle comes from Burdick et al. [2010], and the S model in the mantle comes from Yuan and Romanowicz [2010]. Seismic velocity and Moho topography of Crust 2.0 model [Bassin et al., 2000] is used in the crust. For a detailed description of the algorithm, we refer the reader to Cheng et al. [2016].

Images obtained from classical P -to- S receiver function imaging in a subduction context are usually contaminated by multiple phases reverberating between the surface and the top of the subducted plate [Tauzin et al., 2016], such as PPs and PSs . These free-surface multiples can sometimes generate strong signals, which are mixed together with primary Ps in the migration process. In order to distinguish multiples from primary phases, we first migrate a synthetic data set using a known velocity model and compare the migrated result to the observed model. The synthetic model is intended to represent a subduction zone: it is defined as three volumes of constant velocity (shown in Figure 2b) separated by a Moho at 25 km and a 30° dipping planar interface at greater depth (the slab) as shown in Figure 2b. The interstation spacing is 30 km, and the teleseismic sources used in this study are regularly distributed on a circle around the network, with an average epicentral distance of 80° (Figure 2a). The generation of synthetic waveforms and the process of migration is the same as in Cheng et al. [2016]. As shown in the final migrated image (Figure 2c), the dipping interface is recovered quite well by the migrated primary Ps wave. However, multiple reflected phases are also visible in the deeper part of the model. We identify these multiple signals as PPs and PSs for the dipping structure. The horizontal continental Moho also suffers from spatial aliasing making it difficult to identify, as previously

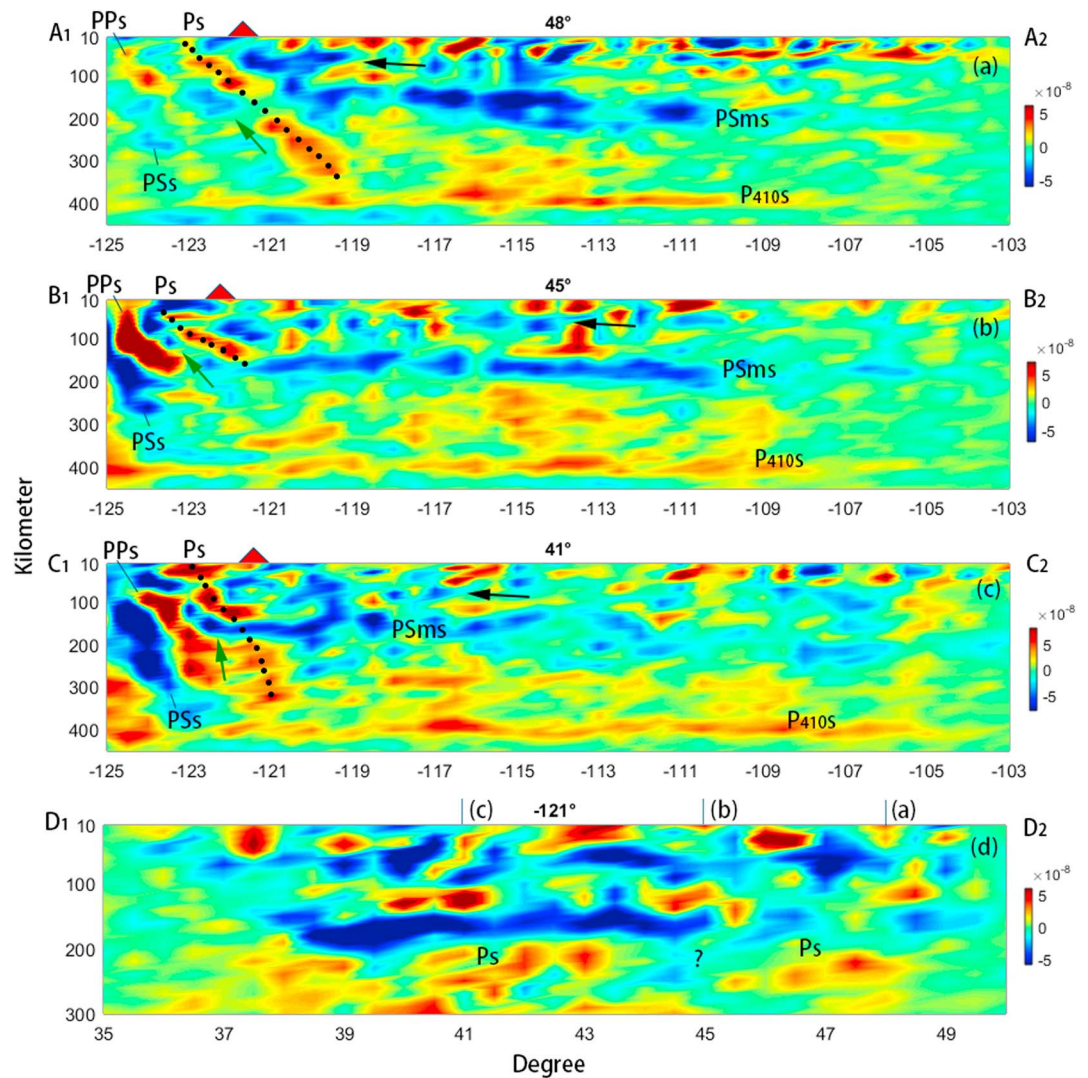


Figure 3. Migrated seismic cross section for (a) A₁-A₂ profile at 48°N, (b) B₁-B₂ profile at 45°N, (c) C₁-C₂ profile at 41°N, and (d) D₁-D₂ profile at 121°W from low-pass-filtered data at 0.2 Hz period. The black dotted line emphasizes the prominent discontinuity related to the slab. The positions of migrated primary signal (*Ps*) and later multiples are labeled on the figures. P410s indicates the 410 km discontinuity. The black arrows in Figures 3a–3c show the continental LAB (blue and discontinuous), the red triangles in Figures 3a–3c show the position of volcanic arc, and the green arrows in Figures 3a and 3b show the oceanic LAB. The question mark in Figure 3d shows the gap in the primary *Ps* arrival.

discussed by Cheng *et al.* [2016]. At the same time, a negative *PSms* reverberation from the continental Moho is clearly imaged around ~100 km depth. Based on this observation, the faint positive signal above the *PSms* phase may therefore represent the *PPms* phase from the continental Moho.

3. Imaging Result

In contrast to the previous CCP model of Tausin *et al.* [2013], where a 3-D image is obtained by interpolating a set of parallel 2-D sections, here we directly present a fully 3-D migrated image of the Cascadia subduction zone. In Figure 3 we show seismic cross sections along three profiles at constant latitude: A₁-A₂ below Northern California, B₁-B₂ below central Oregon, and C₁-C₂ below Washington. The image is obtained from the 0.2 Hz data set. The same images are shown for 0.1 Hz data in Figure S1. The position of the profiles in the map view is showed in Figure 1a. Because of the limited frequency content of the observed seismic wavefield, our model only depicts a low-pass-filtered approximation of the true reflectivity structure.

We highlight two features in this reflectivity model. First, the migration algorithm recovers the 410 km discontinuity approximately as a flat interface near 410 km depth. Second, east of 121°W longitude, a strong negative (blue) signal appears between 150 and 200 km depth. We identify this signal as the *PSms* multiple from the continental Moho that overwhelms the signal associated with the true structure. We interpret this negative signal as a multiple (rather than the base of the lithosphere) for two reasons: first, from the synthetic test in Figure 2, we can see that the *PSms* multiple from a Moho at 25 km is mapped at ~100 km depth; second, the lithosphere-asthenosphere boundary in western North America is expected at around ~80 km depth [e.g., Levander and Miller, 2012; Yuan and Romanowicz, 2010]. Furthermore, we point to the presence of a weak and discontinuous signal at approximately ~80 km on all the profiles (marked by black arrows in Figures 3 and S1), which may represent the bottom of the lithosphere. The lithosphere-asthenosphere boundary (LAB) signal is small and discontinuous at this depth because it suffers from aliasing and the LAB is a relatively weak discontinuity compared to the Moho. Given the station spacing of the U.S. Transportable Array, the same spatial aliasing problem will happen to all structures (Moho and LAB) shallower than ~100 km. Although the negative signal at ~150 km is a multiple from the Moho and should not be interpreted as a discontinuity, it still provides information about shallow structure. For example, in Figures 3 and S1, the apparent depth of the multiple appears to increase east of 112°W, suggesting an increase in thickness of the crust, in agreement with Levander and Miller [2012]. Quantitative interpretation of surface multiples is beyond the scope of this paper and will be subject of future work.

In this study, we focus our attention on one of the major imaged feature: namely, the structure dipping eastward in the upper mantle below the Cascadia volcanic arc, which we relate to the subduction of the Gorda and Juan de Fuca plate. Since the migration suffers from strong multiple signals that generate spurious interfaces in the final image (Figure 2), we first need to separate them from primary phases.

We identify the primary signal *Ps* from multiples in the following way. First, at depths shallower than 100 km, the synthetics (Figure 2) show that dipping interfaces are poorly recovered by primary *Ps* arrival and the multiples accompany the main arrival on the left. Our synthetic example also shows that the red-over-blue signal, which is very strong on the left edge of Figures 3b and 3c, is certainly a multiple. Multiples are identified as *PPs* (red) and *PSs* (blue) after the primary *Ps* (red, highlighted with a black dotted line in Figures 3 and S1). Here we use *Ps* to indicate the first dominant signal transmitted from the dipping slab. In the discussion section, we propose that this signal is the *P*-to-*S* transmitted wave at a discontinuity related to the subducted slab.

Second, this conclusion is further confirmed by comparing our migrated model with the images obtained from a teleseismic *P* wave finite-frequency tomography model [Hawley et al., 2016] (Figures 4 and S2). The *Ps* signals marked by the black dotted lines in Figures 3, 4, S1, and S2 coincide with the upper or middle part of the tomographic fast-velocity anomaly. Furthermore, the green dotted lines in Figures 4 and S2 that we will interpret as the oceanic LAB coincide with the bottom of the tomographic fast-velocity anomaly. Note also that the dipping angle of the slab in the two models coincides with each other. Also, note that the position of the inferred multiples is not spatially coincident with the fast-velocity anomaly of the subducted slab in this tomographic model supporting our interpretation that they are multiples.

In the following sections, we focus our discussion on the 150 km to 410 km depth window, as this portion of the model does not suffer from aliasing problems. In this depth range, the red positive dipping *Ps* signal marked with a black dotted line in Figures 3 and S1 is a *Ps* transmitted wave and represents the dominant seismic discontinuity of the subducted oceanic plate.

The model (Figure 3) shows that the morphology of the Cascadia subduction system varies as a function of the latitude in the upper mantle. A steep subducting slab (~50°) down to at least 300 km is observed for the Gorda plate under Northern California (Figures 3c and S1c), whereas the profile to the north under Washington (Figures 3a and S1a) shows the Juan de Fuca plate gently dipping (~30°) at upper mantle depth. More notable is the absence of *Pms* signal at depths between 150 km and 300 km under central Oregon (Figures 3b and S1b), which leaves a gap in the seismic signature of the subducting plate in this region. Figures 3d and S1d show seismic cross sections along a profile in the longitude direction D₁-D₂, at -121°. In this view, the Gorda plate appears more steeply dipping than the JdF plate to the north with a clear gap in-between, from 43°N to 46°N near ~250 km depth (Figures 3d and S1d).

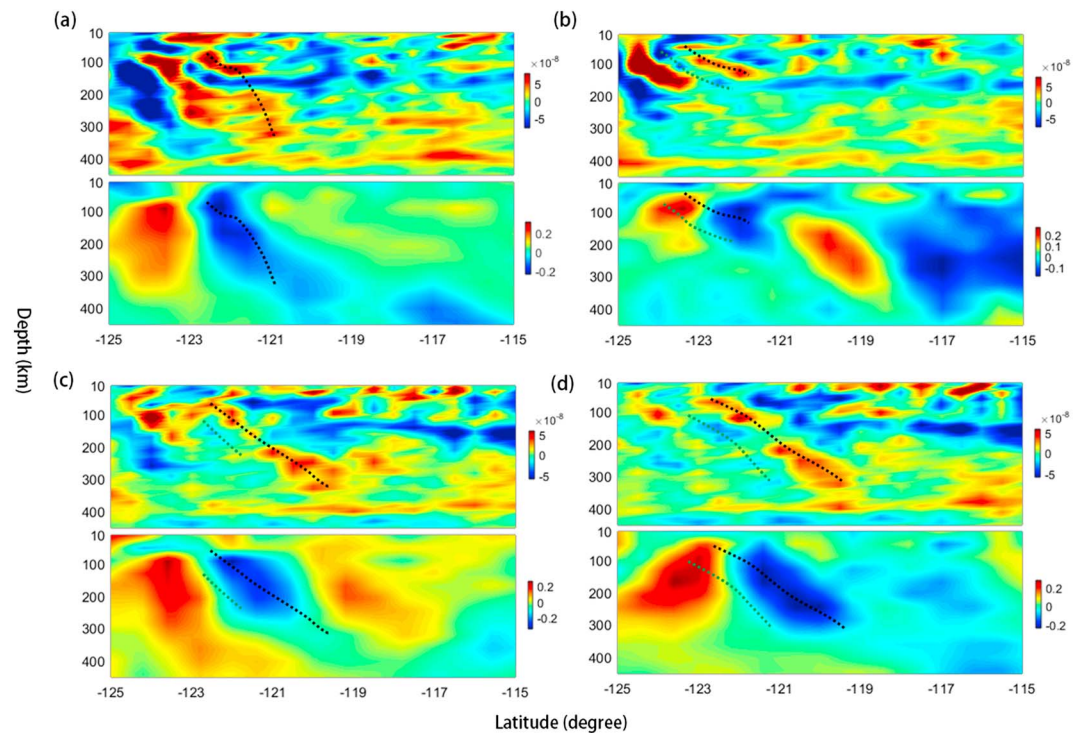


Figure 4. Comparison between our reflectivity model (0.2 Hz data set) (top figure in each pair) and a teleseismic tomography model (bottom figure in each pair) [Hawley *et al.*, 2016] at (a) 41°N, (b) 45°N, (c) 47°N, and (d) 48°N. The black dotted line emphasizes the prominent discontinuity related to the slab as imaged by receiver functions. The green dotted line shows the bottom of the slab from the receiver function study also.

4. Discussion

A variety of processes can perturb the structure of the subducted oceanic plate and modify its seismic expression. Early receiver function studies showed that beneath fore-arc longitudes the structure of the JdF subducted plate is dominated by the presence of an east dipping, low-velocity zone (LVZ), which was first interpreted as the oceanic crust [Langston, 1981]. Some recent models interpret this LVZ as the uppermost layer of the oceanic crust, which has been extensively hydrated before subduction [Bostock, 2013]. Hydration and possibly overpressure [Audet *et al.*, 2009] would result in a strong seismic velocity contrast at the base of the LVZ. Therefore, one possible explanation of our observation of a dipping positive (red) P_s signal in the mid-upper mantle is the expression of a velocity contrast between the LVZ and underlying higher-velocity material in the subducting slab.

However, as a young lithosphere end-member of the global subduction system (6–10 Ma at trench), the oceanic crust is expected to reach the dehydration solidus, *i.e.*, eclogitization, at depth shallower than 100 km [Hacker *et al.*, 2003]. The oceanic crust undergoes eclogitization in a top-down sense leading to gradual disappearance of the LVZ with depth in the subduction zone. Bostock [2013] argues that eclogitization reduces the seismic velocity contrast within the LVZ in two ways. First, the mineralogy changes as lower velocity minerals are replaced by higher-velocity minerals. Second, eclogitization produces an ~10% volume reduction in the solid phase thereby reducing pore pressures. The LVZ under Washington can be traced down to ~100 km; under central Oregon, it disappears at a very shallow depth (~40 km) due to dehydration [Bostock, 2013]. In conclusion, this process occurs before the slab reaches 100 km depth. An observation of the oceanic slab Moho (or base of the LVZ) as deep as ~300 km is therefore quite rare, and the eclogitization process is unlikely to explain our dipping P_s signal in the mid-upper mantle.

Alternatively, another explanation for this signal is that it represents the thermal velocity gradient or boundary layer between the cold subducting slab and the surrounding continental mantle. A similar observation has been made in Southern Central America Cocos plate by MacKenzie *et al.* [2010], where they find a steeply dipping subducting slab down to 200 km under Nicaragua. At 200 km, steady state

thermal models [Peacock *et al.*, 2002] predict a lateral temperature change of around 50°C over a 15–25 km distance. The method of Hacker and Abers [2004] predicts a 6–9% velocity increase from this temperature change in peridotites. Such a broad velocity gradient would be seen as a discontinuity at long wavelengths. Given the resolution of our receiver function data (the 5 s RF data allow a vertical resolution of ~10 km, and the 10 s RF data allow a vertical resolution of ~25 km [Bostock, 1999]), it is hard to distinguish between a thermal gradient layer on this scale and a sharp chemical discontinuity. Given this interpretation, we would also expect to see consistency between our migration model and the longer-wavelength temperature-driven tomographic anomalies observed by Hawley *et al.* [2016].

The heterogeneity of the *Ps* interface along the strike is also intriguing. In our model, the positive (red) dipping *Ps* signal in Figures 3b and S1b under central Oregon disappears by ~150 km depth. However, under Washington and Northern California, this signal persists to the approximate depth of 300 km in the upper mantle. This observation of a gap between 43°N and 46°N is also consistent with the results of tomographic studies [Hawley *et al.*, 2016; Obrebski *et al.*, 2010], showing a much weaker high-velocity anomaly representing the oceanic slab under central Oregon than below Washington or Northern California (e.g., Figure 4b).

It is not clear why the slab signal in both models is not seen past ~150 km depth under central Oregon. Obrebski *et al.* [2010] speculated that the interaction of the Yellowstone plume with the slab, starting from 17 to 19 Ma, caused the breakup of the Cascadia subducting slab and had a longer-lasting effect at the point of origin beneath Oregon. While the arrival of the buoyant plume likely precipitated breakup of the slab, pre-existing weaknesses may also have facilitated this breakup. In our model, the dipping angle varies along strike and is larger under Northern California than under Washington. This change of slab curvature along the trench of the subduction zone could originate from localized deformation due to slab weakening under central Oregon. Bercovici *et al.* [2015] proposed a weakening mechanism for necking and rapid slab detachment, based on grain reduction and damage in polycrystalline rocks due to entrainment of thick buoyant crust such as oceanic plateaux, mid-oceanic ridges, or continental material in the subduction zone. Rheology is also known to play a role in strain localization. We speculate that an alternative mechanism for strain localization and slab-detachment is extensive hydration of the oceanic plate offshore of Oregon due to the presence of faulting through the entire oceanic crust. Such faulting has been proposed based on lithospheric imaging using seismic reflection profiling offshore of Oregon and Washington [Han *et al.*, 2016]. This could lead to the formation of a thick and weak layer of serpentinite in the oceanic mantle.

5. Conclusion

As a conclusion, whatever the causal mechanism is, our migration approach clearly shows a variation in the dip and depth extend of the *Ps* conversion. The observed variation is consistent with that previously imaged using tomographic techniques and is likely caused by a steep thermal gradient between the slab and surrounding mantle rather than a chemical discontinuity. This variability may be related to localized deformation and variations in the hydration of the incoming oceanic lithosphere due to crust-cutting faults observed offshore of Oregon and may also be related to plume processes as previously proposed.

Acknowledgments

This research is supported by the University of California, Berkeley. We thank Robert Martin-Short for the help on improving the quality of the manuscript. Benoit Tauzin and Thomas Bodin were supported by the INSU TelluS program “Imagerie de structures complexes dans le manteau par migration de Kirchhoff.”

References

- Audet, P., M. G. Bostock, N. I. Christensen, and S. M. Peacock (2009), Seismic evidence for overpressured subducted oceanic crust and sealing of the megathrust, *Nature*, *457*, 76–78.
- Audet, P., M. G. Bostock, D. C. Boyarko, M. R. Brudzinski, and R. M. Allen (2010), Slab morphology in the Cascadia fore arc and its relation to episodic tremor and slip, *J. Geophys. Res.*, *115*, B00A16, doi:10.1029/2008JB006053.
- Bassin, C., G. Laske, and G. Masters (2000), The current limits of resolution for surface wave tomography in North America, *Eos. Trans. AGU*, *81*(48), F897.
- Bell, S., Y. Ruan, and D. W. Forsyth (2016), Ridge asymmetry and deep aqueous alteration at the trench observed from Rayleigh wave tomography of the Juan de Fuca plate, *J. Geophys. Res. Solid Earth*, *121*, 7298–7321, doi:10.1002/2016JB012990.
- Bercovici, D., G. Schubert, and Y. Ricard (2015), Abrupt tectonics and rapid slab detachment with grain damage, *Proc. Natl. Acad. Sci. U.S.A.*, *112*, 1287–1291, doi:10.1073/pnas.1415473112.
- Bostock, M. G. (1999), Seismic waves converted from velocity gradient anomalies in the Earth's upper mantle, *Geophys. J. Int.*, *138*, 747–756.
- Bostock, M. G. (2013), The Moho in subduction zones, *Tectonophysics*, *609*, 547–557, doi:10.1016/j.tecto.2012.07.007.
- Bostock, M. G., R. D. Hyndman, S. Rondenay, and S. M. Peacock (2002), An inverted continental Moho and serpentinization of the forearc mantle, *Nature*, *417*, 536–538.
- Burdick, S., et al. (2010), Model update January 2010: Upper mantle heterogeneity beneath North America from traveltimes tomography with global and USArray Transportable Array data, *Seismol. Res. Lett.*, *81*, 689–693.
- Cheng, C., T. Bodin, and R. M. Allen (2016), Three-dimensional pre-stack depth migration of receiver functions with the fast marching method: A Kirchhoff approach, *Geophys. J. Int.*, *205*(2), 819–829, doi:10.1093/gji/ggw062.

- Dahlen, F. A., G. Nolet, and S.-H. Hung (2000), Fréchet kernels for finite-frequency traveltime—I. Theory, *Geophys. J. Int.*, *141*, 157–174.
- Ford, H. A., M. D. Long, and E. A. Wirth (2016), Midlithospheric discontinuities and complex anisotropic layering in the mantle lithosphere beneath the Wyoming and Superior Provinces, *J. Geophys. Res. Solid Earth*, *121*, 6675–6697, doi:10.1002/2016JB012978.
- Gao, H. (2016), Seismic velocity structure of the Juan de Fuca and Gorda plates revealed by a joint inversion of ambient noise and regional earthquakes, *Geophys. Res. Lett.*, *43*, 5194–5201, doi:10.1002/2016GL069381.
- Hacker, B., and G. A. Abers (2004), Subduction factory 3. An excel worksheet and macro for calculating densities, seismic wave speeds, and H₂O contents of minerals and rocks at pressure and temperature, *Geochem. Geophys. Geosyst.*, *5*, Q01005, doi:10.1029/2003GC000614.
- Hacker, B. R., S. M. Peacock, G. A. Abers, and S. D. Holloway (2003), Subduction factory: 2. Are intermediate-depth earthquakes in subducting slabs linked to metamorphic dehydration reactions?, *J. Geophys. Res.*, *108*(B1), 2030, doi:10.1029/2001JB001129.
- Han, S., S. M. Carbotte, J. P. Canales, M. R. Nedimović, H. Carton, J. C. Gibson, and G. W. Horning (2016), Seismic reflection imaging of the Juan de Fuca plate from ridge to trench: New constraints on the distribution of faulting and evolution of the crust prior to subduction, *J. Geophys. Res. Solid Earth*, *121*, 1849–1872, doi:10.1002/2015JB012416.
- Hansen, S. M., K. G. Dueker, and B. Schmandt (2015), Thermal classification of lithospheric discontinuities beneath USArray, *Earth Planet. Sci. Lett.*, *431*, 36–47.
- Hawley, W. B., R. M. Allen, and M. A. Richards (2016), Tomography reveals buoyant asthenosphere accumulating beneath Juan de Fuca plate, *Science*, *353*, 1406–1408, doi:10.1126/science.aad8104.
- Hopper, E., and K. M. Fischer (2015), The meaning of midlithospheric discontinuities: A case study in the northern U.S. craton, *Geochem. Geophys. Geosyst.*, *16*, 4057–4083, doi:10.1002/2015GC006030.
- Langston, C. A. (1981), Evidence for the subducting lithosphere under southern Vancouver Island and western Oregon from teleseismic P wave conversion, *J. Geophys. Res.*, *86*, 3857–3866, doi:10.1029/JB086iB05p03857.
- Levander, A., and M. S. Miller (2012), Evolutionary aspects of the lithosphere discontinuity structure in the western U.S., *Geochem. Geophys. Geosyst.*, *13*, Q0AK07, doi:10.1029/2012GC004056.
- Ligorria, J., and C. Ammon (1999), Iterative deconvolution and receiver function estimation, *Bull. Seismol. Soc. Am.*, *85*, 1395–1400.
- MacKenzie, L. S., G. A. Abers, S. Rondenay, and K. M. Fischer (2010), Imaging a steeply dipping subducting slab in southern Central America, *Earth Planet. Sci. Lett.*, *296*, 459–468.
- Martin-Short, R., R. M. Allen, I. D. Bastow, E. Totten, and M. A. Richards (2015), Mantle Flow geometry from ridge to trench beneath the Gorda-Juan de Fuca plate system, *Nat. Geosci.*, *8*, 965–968.
- McCrory, P. A., J. L. Blair, F. Waldhauser, and D. H. Oppenheimer (2012), Juan de Fuca slab geometry and its relation to Wadati-Benioff zone seismicity, *J. Geophys. Res.*, *117*, B09306, doi:10.1029/2012JB009407.
- Obrebski, M., R. M. Allen, M. Xue, and S.-H. Hung (2010), Slab-plume interaction beneath the Pacific Northwest, *Geophys. Res. Lett.*, *37*, L14305, doi:10.1029/2010GL043489.
- Obrebski, M., R. M. Allen, F. Pollitz, and S. H. Hung (2011), Lithosphere-asthenosphere interaction beneath the Western United States from the joint inversion of body-wave traveltimes and surface-wave phase velocities, *Geophys. J. Int.*, *185*, 1003–1021.
- Peacock, S. M., K. Wang, and A. M. McMahon (2002), Thermal structure and metamorphism of subducting oceanic crust—Insight into Cascadia intraslab earthquakes, *U.S. Geol. Surv. Open-File Rep.*, *02–328*, 123–126.
- Rawlinson, N., and M. Sambridge (2004), Wave front evolution in strongly heterogeneous layered media using the fast marching method, *Geophys. J. Int.*, *156*(3), 631–647.
- Rondenay, S. (2009), Upper mantle imaging with array recordings of converted and scattered teleseismic waves, *Surv. Geophys.*, *30*, 377–405.
- Tauzin, B., R. D. van der Hilst, G. Wittlinger, and Y. Ricard (2013), Multiple transition zone seismic discontinuities and low velocity layers below western United States, *J. Geophys. Res. Solid Earth*, *118*, 2307–2322, doi:10.1002/jgrb.50182.
- Tauzin, B., T. Bodin, E. Debayle, J. P. Perrillat, and B. Reynard (2016), Multi-mode conversion imaging of the subducted Gorda and Juan de Fuca plates below the North American continent, *Earth Planet. Sci. Lett.*, *440*, 135–146.
- Yuan, H., and B. Romanowicz (2010), Lithospheric layering in the North American craton, *Nature*, *466*, 1063–1068, doi:10.1038/nature09332.